Delamination phenomena in aluminum/polyimide deformable interconnects: In-situ micro-tensile testing

Riccardo Lucchini [a], Emanuele Cattarinuzzi [a], Siavash Maraghechi [a], Dario Gastaldi [a], Andrea Adami [b], Leandro Lorenzelli [b], Pasquale Vena [a,c,*]

[a] Department of Chemistry, Materials and Chemical Engineering, Laboratory of Biological Structure Mechanics (LaBS), Politecnico di Milano, Piazza Leonardo da Vinci 32, 20133 Milano, Italy [b] MST — Microsystems Technology Research Unit, Fondazione Bruno Kessler (FBK), Via Sommarive 18, 38123 Trento, Italy
[c] I.R.C.C.S., Via R. Galeazzi 4, 20161 Milano, Italy.

The deformation and failure mechanisms of metal/polymer electrical interconnects with S-shaped planar meanders are investigated. Samples consist of 1 μm thick aluminum conductive coating evaporated on a 10 μm thick polyimide substrate. Uniaxial tensile tests up to 40% stretch with in-situ optical and scanning electron microscopy (SEM) were performed to assess the effects of different meander geometries on the local mechanics. As a consequence of the large strain experienced by the underlying polymeric substrate, two different delamination modes were observed at the metal/polymer interface, namely, (a) shear-based and (b) buckling-based delamination. Mechanisms (a) and (b) are activated depending on the specific meander geometry: interestingly, a crucial role was played by the length of rectilinear arms, which was shown to influence the extent of transverse contraction experienced by the interconnect. Upon increasing stretch, in-situ SEM observations revealed detrimental effects related to the interfacial failure, as metal fracture localizes in the delaminated areas. Experimental results suggest that, in addition to the need of surface treatments aimed at improving the metal/polymer interface adhesion, it is also crucial to conceive optimal geometrical designs to achieve mechanical reliability of stretchable interconnects.

Keywords:
Stretchable electronics
Flexible electronics
Interface delamination
Deformable interconnects
Buckling

1. Introduction

Flexible and Stretchable electronics refer to a new class of devices whose key attribute is the ability to be bent and stretched undergoing large strains (≫1%) keeping their function under mechanical loading as required by the applications. In particular, deformable electrical in-terconnects are pivotal components for large area stretchable and flexible devices, which are conceived as grids of sensing elements whose function is to provide spatially resolved measurements on deformable bodies such as the case of applications in the biomedical field [1,2,3]. Nevertheless, matching the mechanical response of the metal film and the polymeric substrate still opens some issues related to functional failure [4,5,6]: to address the associated challenges in material science, it is instrumental to improve the mechanical reliability and hence the electrical functionality [7] of deformable interconnects. Cracking of the metal films and interface delamination phenomena represent the

most critical mechanical issues for metal/polymer systems. In particular, previous studies have shown that in metal/polymer systems subject to stretching, the metal film first develops cracks perpendicular to the ten-sile direction at low strains [8,9]. Upon further loading, compressive transverse stresses arise in the film strips due to a Poisson's ratio mismatch between the substrate and the film, causing delamination and buckling in a direction perpendicular to the tensile direction [10,11,12, 13]. As the metal film delaminates and becomes freestanding, the benefits related to the interaction with the compliant substrate are lost; in-deed, experiments have shown that a freestanding thin metal film usually fractures at a smaller strain with respect to thin metal films bonded to a polymeric substrates [14,15,16]. The low ductility of a free-standing metal film results from local thinning. For a sufficiently thin film with exposed free surface, dislocations readily escape from the sur-face [17,18]. Subsequently, the metal does not harden appreciably and even a small perturbation in the metal film thickness promotes necking formation. Although metal cracking and buckling induced by transverse compression have been widely reported in literature, these studies generally refer to fully coated metal/polymer systems and hence they do not provide a comprehensive knowledge on patterned metal films onto polymeric substrates, which are the leading choice for deformable interconnects developed by microfabrication technologies. In the coplanar technology [19,20], in fact, the deformability of the device is

 * Corresponding author at: Department of Chemistry, Materials and Chemical Engineering, Laboratory of Biological Structure Mechanics (LaBS), Politecnico di Milano, Piazza Leonardo da Vinci 32, 20133 Milano, Italy.

   E-mail addresses: riccardo.lucchini@polimi.it (R. Lucchini), emanuele.cattarinuzzi@polimi.it (E. Cattarinuzzi), siavash.maraghechi@mail.polimi.it (S. Maraghechi), dario.gastaldi@polimi.it (D. Gastaldi), andadami@fbk.eu (A. Adami), lorenzel@fbk.eu (L. Lorenzelli), pasquale.vena@polimi.it (P. Vena).

achieved by means of stretchable interconnects able to withstand the high deformations requested by the specific applications. Metal inter-connects featuring suitably designed geometry have been explored, proposing different structural designs [4,21], among which S-shape geometry has been widely used [22,23,24,25]. This approach is, up to date, one of the most promising strategies to achieve extremely large strains (>200%), accommodated by the meander in-plane bending [26], with constant and high conductivity, depending on the selected materials ($35 \div 60 \cdot 10^6$ S/m) [27,28]. Several recent studies addressed new breakthroughs in the mechanical reliability of metal/polymer systems, providing increasing knowledge on the specific issues of patterned deformable interconnects [4,29,30,31,32]. Numerical analysis on the deformation behavior of S-shaped interconnects allowed to interpret experimental evidences of extreme stretchability by means of solid me-chanics arguments [33,34]: upon stretch of the polymeric substrate, the meandering structure causes the strain field to become non-homogeneous nearby the interconnect, relieving most of the stresses experienced by the metal conductor. Normally, this mechanism postpones metal fracture, thus extending the effective stretchability of the device. Nevertheless, combined experimental and numerical studies [5] have shown that, though stress peaks do not trigger the development of cracks in the metal, they may concentrate at the metal/polymer interface and go beyond critical tractions, leading to interfacial delamination. Naturally, the non-homogeneous stress distribution greatly depends on the interconnect geometry, which thus dictates whether and where delamination may occur. In this paper the local deformation mechanism of aluminum/polyimide deformable S-shape electrical interconnects subjected to uniaxial tensile stretch, characterized by a moderate stiffness mismatch ($E_{Al}/E_{PI} \sim 20$), have been investigated. The local mechanics of this material system is suitable to investigate the issue of stretch-induced metal/polymer delamination, which is well reported in the literature [35,36]. Accordingly, we present an experimental study which explores the deformation modes and associated mechanical failures of stretchable aluminum/polyimide interconnects; the study is carried out by means of tensile tests with in-situ SEM as well as optical imaging. The role of the geometrical design of the S-shaped aluminum meanders is discussed. Finite element models have been used to support the inter-pretation of experiments on a solid mechanics basis. The results reveal a correlation between the specific meander geometry and the failure mechanisms experienced by the interconnect. Design rules to enhance the reliability of deformable interconnects can be inferred from the spe-cific results achieved in this work.

2. Experimental

Fabrication of devices was performed on Si 4″ substrates, single side polished. Doping and crystal orientation were not considered since wa-fers were used only as mechanical support during fabrication. In order to provide a repeatable adhesion of layer on wafers, a thin oxide layer (30 nm) was grown by thermal dry oxidation and treated with plasma oxygen before coating with the structural layer (Matrix Plasma Asher, power 200 W, O_2 1.5 Torr, temperature 80 °C, time 1′ and 20″). The sub-strate (structural layer) was implemented with a polyimide film, Durimide DI115A, with a target thickness of 10 μm. In order to reduce the layer adhesion and allow the removal of devices from the SI sub-strate at the end of the process, wafers were treated with a primer be-fore deposition, since the composition DI115A already includes a primer and further priming is reported to reduce the adhesion in the re-sist datasheet. The polyimide film was then spun with spread at 700 rpm for 4 s, sit step 10 s, spinning at 1000 rpm for 45 s. Then, soft bake was performed on hotplate in two steps for 2 min at 100 °C, and 5 min at 135 °C. Final bake of structures was performed at 350 °C for 1.5 h in order to provide the full mechanical properties of the material. Generally polyimide represents one of the material selections for de-formable electronics applications with useful properties such as chemi-cal and radiation resistance, electrical performance and mechanical

stability. Its high elastic modulus and its capability to undergo large permanent deformations make it a suitable candidate as a supporting material for flexible or stretchable electronic devices. In contrast to other widely used polymers which exhibit higher compliance and elas-tic recoil such as PDMS, the higher stiffness of polyimide provides a better confinement and mechanical shielding for the conductive metal layers [37,38]. The metal layer was deposited by evaporation of 1 μm of aluminum (e-gun evaporation, ULVAC high vacuum coater EBX-16C) and defined by lift-off in a planar S-shape design. For this purpose, the deposition of the layer was performed after coating the wafer with Ma-N 1420 negative resist with thickness 2100 nm, followed by layer lithography and development. In order to enhance the Al adhesion to the substrate, the surface of the polyimide was activated before Al depo-sition with a further oxygen plasma treatment as already described above. Lift-off was performed with DMSO at 80 °C in ultrasound bath until removal was complete. The geometrical design of the interconnects is characterized by three parameters: the meander radius (R), amplitude (A) and width (W). Five different sets of the geometrical parameters have been investigated (See Table 1).

The length of the rectilinear arm A_{in} is also reported in Table 1 as it will be a parameter with mechanical relevance. Fig. 1 shows a represen-tative sample in which the polyimide substrate and two S-shaped alu-minum metal lines are visible. The devices were separated by dicing saw cutting, setting the cut depth slightly above the polyimide thickness in order to preserve the substrate integrity.

The nominal width and length of the samples were of 1.3 mm and 15 mm, respectively. The gauge length of the serpentines samples was 5 mm; furthermore, 5 mm per side has been devoted to gripping area. Micro-tensile testing with simultaneous imaging of the samples has been carried out by means of an in-house developed micro-tensile equipment (featuring a 5 N load cell and a displacement actuator with a resolution of 50 nm) with vacuum proof components, suitable for the use in SEM chamber. Optical (Olympus LEXT OLS4100, confocal Laser Scanning Microscope) and SEM (Zeiss EVO 50 EP, LaB$_6$ electron gun) observations have been performed during stretching of the interconnects. Displacement driven tests have been performed, at room temperature. Preliminary tests have been carried out with the purpose to assess suitable loading rates and maximum applied stretch since, differently from other polymers, polyimide exhibits a visco-elasto-plastic mechanical behavior [39,40,41], undergoing a smooth and gradual transition from the linear elastic to the irreversible (plastic like) regime [42]. Based on these preliminary tests, a displacement rate of 1 μm/s was selected in order to minimize the time-dependent contributes to the mechanical response, which would have affected the reliability of the in-situ analysis procedure.

The mechanical characterization of the single constituents alumi-num and polyimide was also achieved, with the purpose to provide suitable material constitutive laws in the finite element models which simulate the stretching process. The polyimide was characterized through uniaxial tensile tests performed by means of the micro-tensile equipment described above. The sample size and testing parameters are the same as that of the aluminum/polyimide samples. A direct characterization of the aluminum layers could not be achieved, as standalone material samples do not exist. Aluminum layers evaporated on Si substrates having a thickness comparable to that of the

Table 1
Geometrical parameters for the tested S-shaped interconnects.

| Distance within meanders	Width	Radius	Amplitude	Sample identifier
A_{in} [μm]	W [μm]	R [μm]	A [μm]	
30	10	20	90	W10R20A90
50	10	40	150	W10R40A150
40	20	20	120	W20R20A120
60	20	40	180	W20R40A180
90	50	40	270	W50R40A270
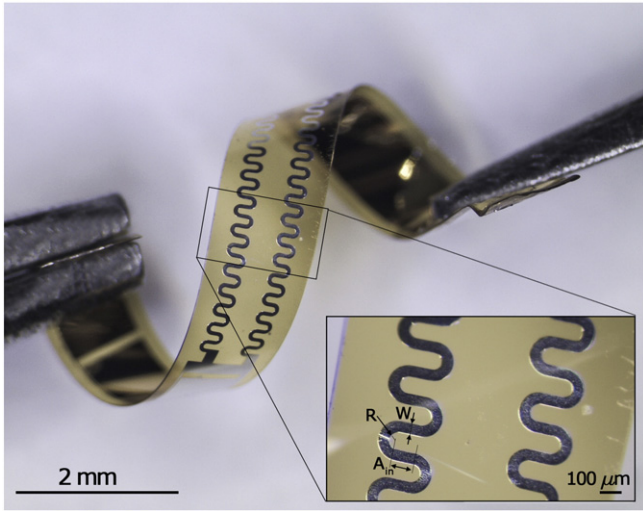
Fig. 1. S-shaped deformable interconnect sample. Three main parameters defining the S-shaped geometry are highlighted in the inset: rectilinear arm (A_{in}), width (W) and radius (R).

interconnects were characterized by means of nanoindentation testing. To this purpose, a spherical indenter with 25 µm tip radius was used [41]. The elastic modulus was obtained through the Field and Swain procedure [43]; while, yield stress and work hardening were estimated through hardness measurement as suggested by Tabor [44].

3. Results

The stress versus strain data for polyimide samples and for aluminum/polyimide samples are reported in terms of nominal or engineering stress versus nominal strain. The stress vs strain data, reported in Fig. 2, show that the overall mechanical response was insensitive to the geometrical features of the interconnects, resulting in a global behavior that was dominated by the non linear stress vs strain response of the polymer. In particular, all samples exhibited an initial elastic moduli of approximately 3.2 GPa; while, a decrease of the tangent modulus is observed for strain larger than 10%.

This is an expected result as the cross sectional area of the metal layer is three orders of magnitude lower than the cross sectional area
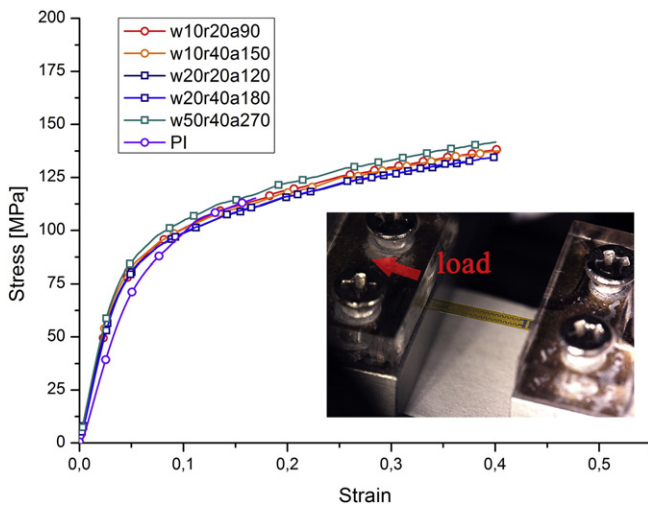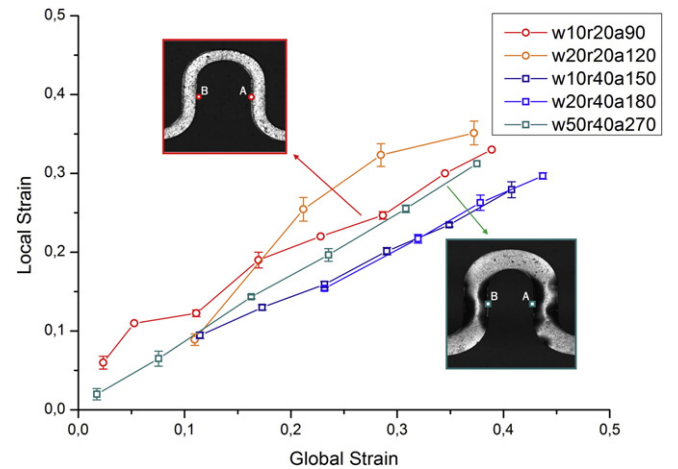
of the polymer, whereas the Young modulus of the metal is only one order of magnitude higher than that of the polymer. However, although the macroscopic mechanical response of all interconnects was similar, local (micro) deformation modes can be greatly affected by the meander geometry, with a non-negligible effect on the mechanical reliability of the system. An optical analysis during the micro-tensile tests has been conducted with the purpose to quantify the deformation mechanisms at local level. To this aim, a measure of the in-plane local distortion has been defined as the nominal strain of the material line connecting the opposite points A and B on the metal coatings (Fig. 3):

$$\text{Local strain} = \frac{(B-A)_t - (B-A)_{t_0}}{(B-A)_{t_0}} \tag{1}$$

in which $(B - A)$ is the length of the line segment which connects the points A and B reported in Fig. 3; while, the subscripts t_0 and t refer to the initial and current length of the line segment, respectively.

A comparison between the in-plane distortions for all sample geometries is reported in Fig. 3, where differences in the local behavior can be appreciated: in particular, samples w10r20a90 and w20r20a120 (red and orange curves in Fig. 3) show a higher local strain with respect to the other designs. Furthermore, the in-situ optical analysis suggests a correlation between the amount of the local strain and the occurrence of stretch-induced delamination. The optical images insets in Fig. 3 are representative examples of optical light reflections in the deformed configurations. These indicate possible damage or delamination and out of plane buckling for samples w10r40a150, w20r40a180 and w50r40a270, i.e., those exhibiting lower local strain with respect to the remaining samples. Whereas samples undergoing larger local strain (i.e., w10r20a90 and w20r20a120) did not exhibit delamination, sug-gesting that these two designs can better accommodate the overall ap-plied strain. Noteworthy, it was observed that delaminations and out of plane buckling mostly occurred for the layouts featuring longer rectilin-ear arms, thus suggesting the layout parameter A_{in} to play the most relevant role as concerns the influence of the S-shaped design on the local mechanical response. To gain insights into the stretch-induced failure phenomena evidenced by the optical analysis, in-situ tensile tests within the Scanning Electron Microscope (SEM) chamber have been carried out. Surface morphology was obtained by means of secondary electrons (SE) micrographs. The edge effect (i.e., the higher emission of secondary electrons at edges of morphological features [45]), en-hances the image contrast, making edge regions appear brighter. This effect is exacerbated when out of plane displacements occur. For instance, when a delaminated metal coating lifts up, it causes the crests of delaminated regions to appear brighter. This makes SE detection a

Fig. 2. Stress vs strain curves (nominal thickness, 10 µm, nominal width, 1.3 mm) as obtained from the uniaxial tensile tests; in the inset, a representative sample fixed between the grippers is reported.

Fig. 3. Comparison between global and local strain (Eq. (1)) measured through optical analysis. Two representative stretched meanders, as obtained through the optical imaging, are reported in the insets; A and B represent the points used to estimate the local strain.

suitable technique to provide a visual representation of the delaminated area, besides allowing to identify local failures (e.g., metal fracture) at a characteristic length scale beyond the resolution power of an optical mi-croscope. For each interconnect, monotonic loading programs were ap-plied within the SEM chamber. Loading rates and maximum applied stretches were the same as those applied under optical observation tests. Tests were carried out until failure, which occurred at about 48.8 ± 7.4% applied stretch. The test was stopped for about 60 s at each 200 μm displacement increment with the purpose to acquire high resolution images at a given global stretch level. Based on the pre-liminary mechanical characterization, the aforementioned time lapse was assumed to be short enough to avoid viscoelastic artifacts that can influence the deformed configuration. SEM images revealed that, in-deed, delamination also affected the samples featuring higher local strains in previous analysis (e.g., w10r20a90, Fig. 4).

Interestingly, in this case a uniform shear failure at the edge of the metal/polymer interface was observed (Fig. 4a,b, left panel), which explains the absence of appreciable out of plane displacement of the metal film and the related uncapability to detect the phenomena at the optical microscope. SEM data confirmed the buckling phenom-ena observed through the optical microscope. In particular, the buck-ling phenomena occurred for designs having A_{in} longer than 40 μm. Indeed, by visual inspection of the SEM images, interconnects w10r20a90 and w20r20a120 (A_{in} equal to 30 and 40 μm, respective-ly) exhibited uniform shear dominated delamination. On top left panels of Fig. 4, details of the two samples with A = 90 μm (A_{in} equal to 30 μm) and A = 120 μm (A_{in} equal to 40 μm) are reported. A roughly uniform delamination along the edge of the metal line has been found (insets refer to stretch level of about 40%); this metal/polymer detachment is generated by shear stress at the inter-face and no out of plane buckling has been found, in agreement with the outcome of the tensile tests carried out under the optical micro-scope. The right panels of Fig. 4 show details of samples featuring $A_{in} > 40$ μm, focusing on the regions in which the out of plane displacement of the metal coating did localize.

In-situ testing performed in SEM also provided insights into local failure phenomena occurring after delamination. In particu-lar, Fig. 5 shows the buckled aluminum film; the inset shows a fracture in the metal layer occurring at the boundary edge of the delaminated area.

Fig. 5. SEM image of a buckled metal meander; in the inset, a crack localized on the buck-led aluminum is highlighted.

4. Discussion

The results presented in this work outline two different deformation mechanisms upon axial stretch for different S-shaped designs, as illustrated in Fig. 6. The left panel of Fig. 6 depicts the shear-based delamination found for the samples with $A_{in} \leq 40$ μm. Bold red arrows show the axial stretch applied to the sample; small red arrows denote contraction of the sample along the direction perpendicular to that of stretching.

Shear stress acting at the metal/polymer interface induced by the axial stretching causes shear-based detachment of the metal coating. The right panel of Fig. 6 shows the buckling-based delamination found for samples with $A_{in} > 40$ μm. Small red arrows show the axial stretching applied on the samples; bold red arrows show the contraction of the sample along the direction perpendicular to the stretching direction. The latter induces compression on the metal layer, eventually leading to delamination and out of plane buckling only for samples $A_{in} > 40$ μm. Optical microscopy allowed to deter-mine an approximate value of the critical axial stretch at which out of plane buckling occurs; it was estimated to be around 12% global axial strain ($\varepsilon_{axial}^{cr} \sim 12\%$). Moreover the change in the meanders amplitude A, i.e. the transverse serpentine shortening (ε_A), has been measured during the experimental tests through confocal laser microscopy. Fig. 7 shows the comparison between the two extreme geometries: $A_{in} = 30$ μm and $A_{in} = 90$ μm.
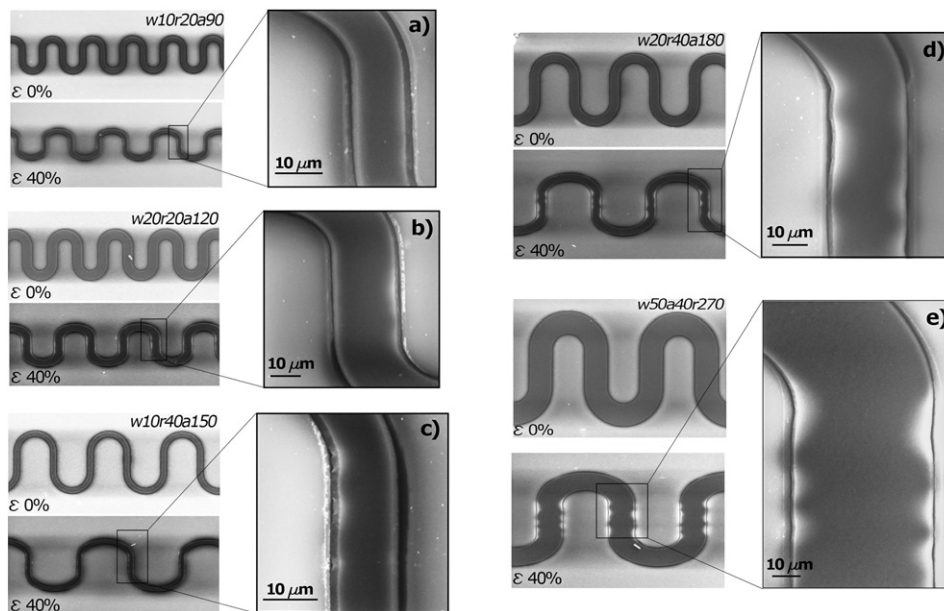

Fig. 4. SEM images of the tested samples upon stretch at two magnification levels. The images on 1st and 3rd columns report the undeformed and deformed interconnects at 40% strain; the images on 2nd and 4th columns report a magnification view that allows at identifying the delaminated regions (bright area).
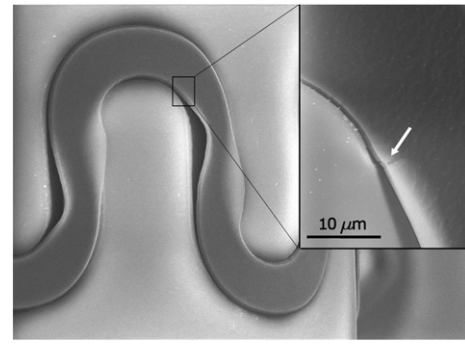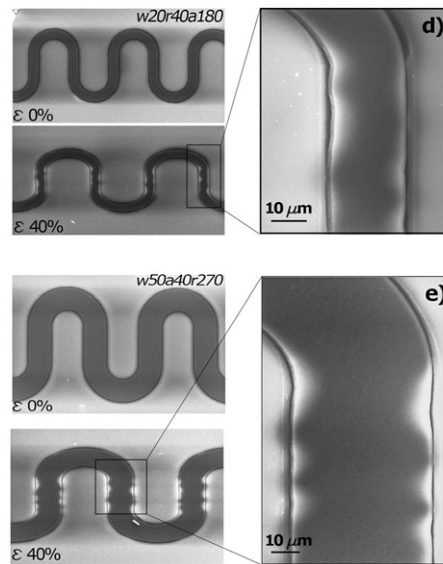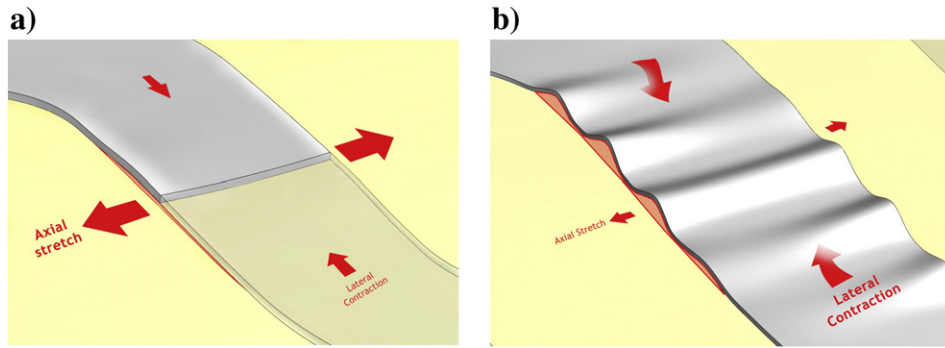
Fig. 6. Delamination mechanisms. (a) Shear-based: the delamination is driven by the axial stretch which induces shear at the metal/polymer interface; (b) buckling-based: the contraction along the direction perpendicular to the loading direction induces compression in the metal coating and eventually buckling.

At a given applied axial stretch, larger meanders (w50r40a270) are subjected to higher compressive strains as compared to sample w10r20a90 (see Fig. 7). The two samples reported in Fig. 7 are represen-tative for the two deformation mechanisms identified in this work. Higher transverse contraction experienced by w50r40a270, even at the early stage of the loading program, indicates that out of plane buckling is more likely to occur for this specific sample as compared to other samples with smaller A_{in}. This is consistent with the finding of this work.

A finite element model has been set up with the purpose to estimate the transverse compressive strain exhibited along the vertical arm of the serpentine geometry.

To this aim, the commercial finite element solver ABAQUS (Dassault Systèmes Simulia©, Providence, RI, US) was used. A full three dimensional model consisting of approximately $3 \cdot 10^5$ hexahedral trilinear solid elements was developed to simulate a representative unit featuring two complete meanders of the whole sample (Fig. 8). Static analyses have been performed by applying a displacement-based boundary conditions consistent with a macroscopic maximum strain of 20%. The geometric features of the samples allowed to introduce boundary condi-tions as follows: i) symmetry has been imposed along the median line of the sample by constraining the displacement component perpendicular to the symmetry plane; ii) periodic boundary conditions have been ap-plied on the two vertical edges of the two meanders region. Periodicity conditions have been applied to the displacement components at all the nodes of the left and right surfaces of the finite element model: this was done automatically by means of an in-house developed Python script. These boundary conditions constrain the two corresponding boundaries to experience the same strain and opposite stress, meanwhile allowing

to catch stress, strain and displacement fluctuation at the small scale, in analogy to what happens in the real samples. The aluminum was modeled as a von Mises elastic plastic isotropic material with work hardening. Young modulus (69 GPa) and yield stress vs plastic strain are those obtained through the characterization study [41]. The polyimide was also modeled as an isotropic elastic–plastic material with Young modulus (3.2 GPa) and yield stress as obtained through the micro-tensile tests [41]. The elastic–plastic modeling of polyimide is a phenomenological approach suited for polymers exhibiting permanent strain upon stretching, as it happens for the polyimide (data not shown)[38]. Viscoelastic effects in the polymer material were not included in the constitutive models as major deformation mechanisms resulting from the polyimide/aluminum interaction were sought. A perfect bonding between the polymer substrate and the metal coating was considered as the aim of the model was not to reproduce the delamination phenomena itself, while to gain insights on the deformation modes
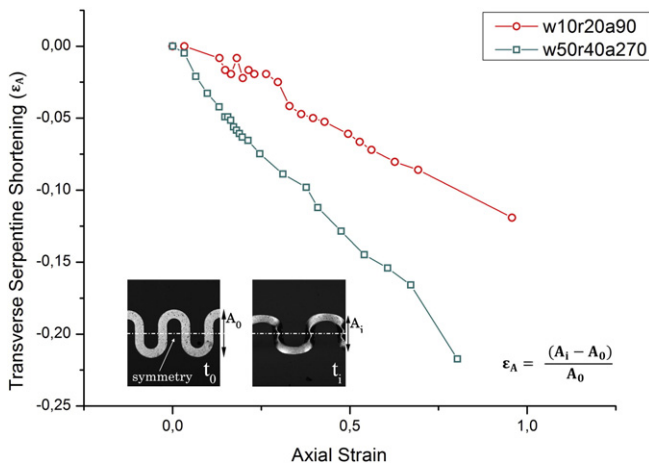
Fig. 7. Transverse shortening of the serpentine. In the inset the quantity ε_A is represented on the largest interconnect ($A_{in} = 90\ \mu m$).

$$\varepsilon_A = \frac{(A_i - A_0)}{A_0}$$
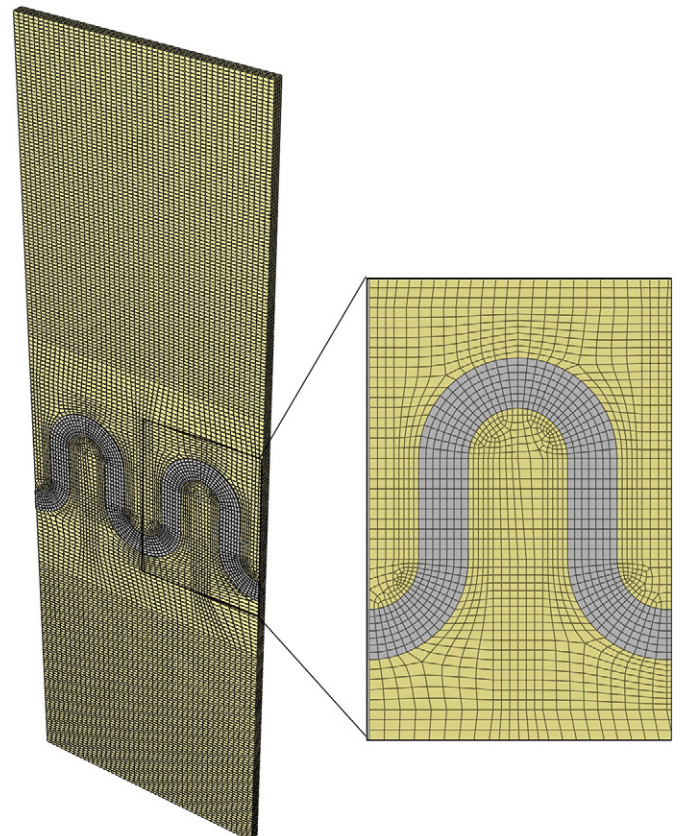
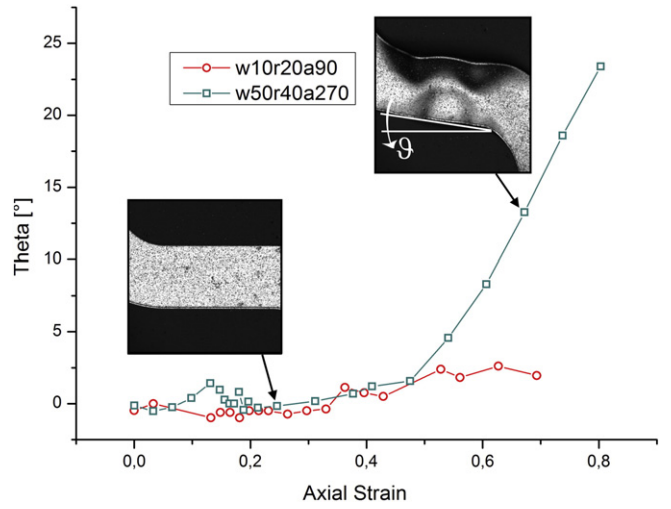**Fig. 8.** Finite element discretization of a unit cell of the stretchable interconnect.
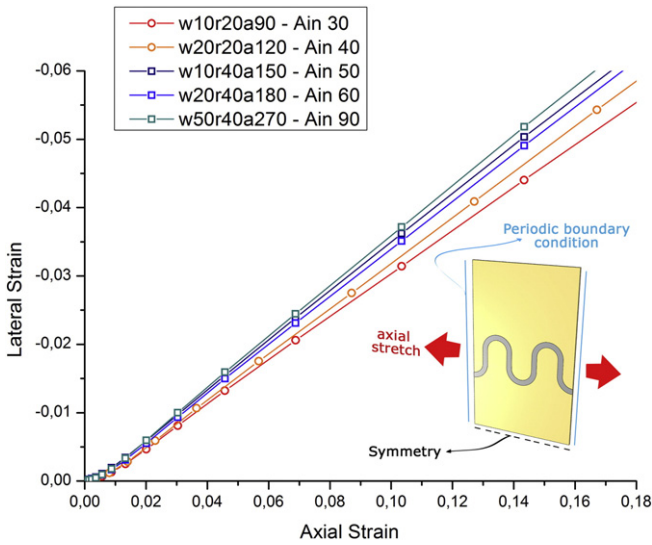
Fig. 9. Compressive strain along the direction perpendicular to the loading direction on the rectilinear arm vs applied axial strain; strains are calculated by means of finite element models. The comparison between the five different geometries highlights an increasing compressive strain for increasing A_{in} value. Applied boundary conditions are represented in the inset.

Fig. 11. Angle of rotation from the initial configuration of the rectilinear arm in the metal coating. The evolution of the angle θ with respect to the axial stretch shows a different mechanical deformation behavior of the S-shape interconnects that can be related to the occurrence of the buckling phenomena.

leading to the onset of the interface delamination; on the other hand, more refined numerical models aimed at describing the whole process until complete failure will be developed in a future study.

The obtained finite element model has been validated by comparing the macroscopic stress vs strain response in the axial direction to the experimental data [40].The finite element analyses provided an estimate of the transversal contraction of the samples upon axial stretching. Compressive strain of the polymeric substrate along transverse direction results in compressive strain along the rectilinear arm of the bonded metal coating. It can be shown that the geometrical parameter A_{in} plays the most relevant role; indeed, for increasing values of A_{in}, the metal experiences an increasing compressive strain (see Fig. 9 in which transverse metal strain vs axial strain is reported).

The compressive strain along the rectilinear arm of the metal coating, measured through optical images analyses, at the onset of buckling on the sample with $A_{in} = 90$ μm is about 5%. Finite element analysis results show that the compressive strain of 5% for $A_{in} = 90$ μm corresponds to about 14% axial stretch (see green line in Fig. 9). This value is slightly larger than the critical axial stretch estimated through the ex-periments ($\varepsilon_{axial}^{cr} \sim 12\%$). At the same axial stretch level, the samples with $A_{in} = 30$ μm exhibited a computed compressive strain in the metal of about 4.2% (15% lower than that found in buckled samples), as represented in Fig. 9 with the red line.

As concerns the stress field computed by the FEA, the influence of the interconnect geometry can be better explained when comparing de-signs featuring equal width: i) samples w10r40a150 and w20r40a180 experienced higher compressive stresses and lower shear stresses as compared to their counterparts featuring equal width and shorter rectilinear segments (w10r20a90 and w20r20a120, respectively. See Fig. 10); and ii) consistently, experimental data show that samples w10r40a150 and w20r40a180 exhibited buckling along the edges of the rectilinear segments, while samples w10r20a90 and w20r20a120 failed by uniform shear-delamination.

The extensive delamination and out of plane buckling occurring on samples exhibiting larger A_{in} is such that the mechanical constraint provided by the interaction with the substrate is lost allowing for substan-tial rotation of the rectilinear arm as the axial stretch increases. Fig. 11 shows that, at the early stage of the loading program, the proper con-straint of the substrate on the metal layer prevents rotation of the recti-linear arm; whereas, upon delamination and buckling of w50r40a270, a substantial increase of the arm rotation occurs as metal/polymer inter-face stress has been released. This will cause further in-plane bending of the curvilinear meander with further delamination which eventually may lead to metal cracking. Geometric compatibility between metal coating and substrate is found on the samples with shorter A_{in} (such as w10r2a90) up to 70% axial stretch. This is shown by the smaller rota-tion of the rectilinear arms found in this latter sample. This finding would suggest that this specific geometry would decrease the probabil-ity of failure upon stretching.
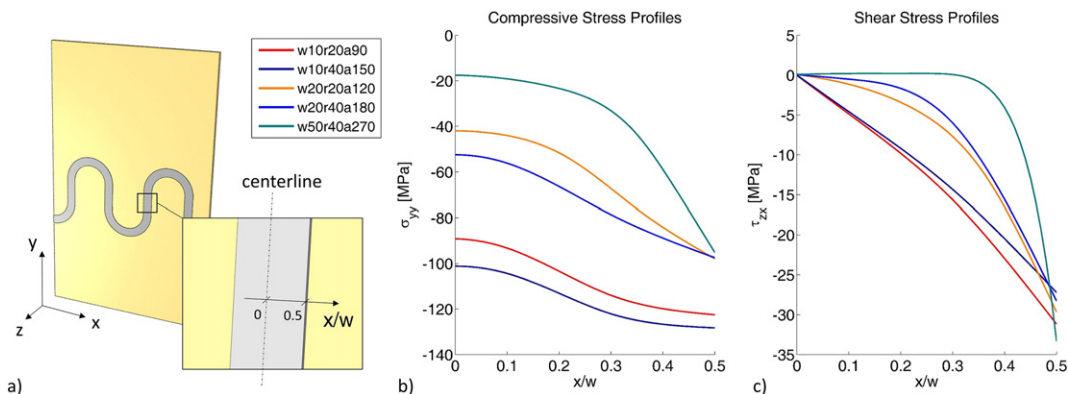
Fig. 10. (a) Schematic illustration of the normalized profile coordinate, x/w, along the half width; (b) compressive stress profiles and (c) shear stress profiles.

Buckling and delamination phenomena have been largely studied on metal coating/polymer composites with emphasis on fully coated systems. Both buckling-based [10,11,12,13] and shear-based delamination have been investigated [45,46]. On the other hand, mechanical failure in stretchable metal/polymer patterned interconnects have been considered on material systems different than that studied in the present work, with specific reference to lateral fibrillation of PDMS/copper systems [5,35,36] and to plastic strain accumulation on the metal components using models with perfect metal/polymer interfaces [4,29,34]. The present study matches the interface failure behavior with the layout geometry of deformable interconnects, and therefore provides an innovative contribution as concerns the relationship between structural design and mechanical reliability of S-shaped interconnects.

5. Conclusion

In this paper, deformation mechanisms of metal/polymer interconnects have been investigated through a combination of micro-tensile testing and in-situ optical and SEM imaging. Two main stretch-induced failure mechanisms have been outlined: a) shear-based and b) buckling-based metal/polymer delamination. The experiments have shown that the occurrence of mechanism a) or b) is related to the geometrical design of the S-shaped interconnects. In particular, the rectilinear arm length, A_{in}, was identified as a key parameter: samples with the longest A_{in} exhibited out of plane buckling, whereas other samples experienced shear-based delamination. Buckling of the metal film along the rectilinear arm is induced by the compressive stress of the metal owed to transverse contraction of the polymeric substrate upon axial stretch. Numerical analyses allowed to elucidate a correlation between the extent of lateral contraction and A_{in}, providing indications for the in-terpretation of experimental results on a solid mechanics basis. Delamination of the metal/polymer interface is a failure mode of practical relevance in the field of deformable interconnects. Indeed, delamination will cause loss of the confinement effect granted by the substrate, leading to a free-standing metal film, which is more prone to fracture onset and propagation as already pointed out in discussing Fig. 5.

In this work, the effect of geometrical features of the aluminum meanders have been investigated; while process parameters, including bonding enhancement surface treatments, were kept unchanged for all samples. The presented results provide useful indications on the correlation between geometrical features and relevant deformation mechanisms that can jeopardize the mechanical and hence electrical reliability of the deformable interconnects; therefore, these results can set the basis for an optimal shape design of the interconnects. Once optimal geometrical criteria are set, further studies aiming at optimizing inter-face bonding should be undertaken.

Acknowledgments

References

[1] D.-H. Kim, N. Lu, R. Ghaffari, Y.-S. Kim, S.P. Lee, L. Xu, J. Wu, R.-H. Kim, J. Song, Z. Liu, J. Viventi, B. de Graff, B. Elolampi, M. Mansour, M.J. Slepian, S. Hwang, J.D. Moss, S.-M. Won, Y. Huang, B. Litt, J.A. Rogers, Materials for multifunctional balloon catheters with capabilities in cardiac electrophysiological mapping and ablation therapy, Nat. Mater. 10 (4) (2011) 316–323 (URL http://dx.doi.org/10.1038/nmat2971).

[2] D.-H. Kim, J. Viventi, J.J. Amsden, J. Xiao, L. Vigeland, Y.-S. Kim, J.A. Blanco, B. Panilaitis, E.S. Frechette, D. Contreras, D.L. Kaplan, F.G. Omenetto, Y. Huang, K.-C. Hwang, M.R. Zakin, B. Litt, J.A. Rogers, Dissolvable films of silk fibroin for ultrathin conformal bio-integrated electronics. Nat. Mater. 9 (6) (2010) 511–517, http://dx.doi.org/10.1038/nmat2745 (URL http://dx.doi.org/10.1038/nmat2745).

[3] L. Xu, S.R. Gutbrod, A.P. Bonifas, Y. Su, M.S. Sulkin, N. Lu, H.-J. Chung, K.-I. Jang, Z. Liu, M. Ying, C. Lu, R.C. Webb, J.-S. Kim, J.I. Laughner, H. Cheng, Y. Liu, A. Ameen, J.-W. Jeong, G.-T. Kim, Y. Huang, I.R. Efimov, J.A. Rogers, 3D multifunctional integumenta-ry membranes for spatiotemporal cardiac measurements and stimulation across the entire epicardium, Nat. Commun. 5 (2014) 3329, http://dx.doi.org/10.1038/ncomms4329.

[4] M. Gonzalez, F. Axisa, M.V. Bulcke, D. Brosteaux, B. Vandevelde, J. Vanfleteren, Design of metal interconnects for stretchable electronic circuits, Microelectron. Reliab. 48 (6) (2008) 825–832 (URL http://www.sciencedirect.com/science/article/pii/S0026271408000760).

[5] Y.-Y. Hsu, M. Gonzalez, F. Bossuyt, F. Axisa, J. Vanfleteren, I.D. Wolf, The effect of pitch on deformation behavior and the stretching-induced failure of a polymer-encapsulated stretchable circuit, J. Micromech. Microeng. 20 (7) (2010) 075036 (URL http://stacks.iop.org/0960-1317/20/i=7/a=075036).

[6] T. Li, Z. Suo, S. Lacour, S. Wagner, Compliant thin film patterns of stiff materials as platforms for stretchable electronics, J. Mater. Res. 20 (12) (2005) 3274–3277 (URL http://www.scopus.com/inward/record.url?eid=2-s2.0-3044 4461021 partnerID=40 md5=517f588271dd98e80918fabb11eedff6).

[7] T. Adrega, S.P. Lacour, Stretchable gold conductors embedded in PDMS and patterned by photolithography: fabrication and electromechanical characterization, J. Micromech. Microeng. 20 (5) (2010) 055025 (URL http://stacks.iop.org/0960-1317/20/i=5/a=055025).

[8] B. Erdem Alaca, M. Saif, H. Sehitoglu, On the interface debond at the edge of a thin film on a thick substrate, Acta Mater. 50 (5) (2002) 1197–1209 (URL http://www.sciencedirect.com/science/article/pii/S13596 45401004219).

[9] N. Lambricht, T. Pardoen, S. Yunus, Giant stretchability of thin gold films on rough elastomeric substrates, Acta Mater. 61 (2) (2013) 540–547 (URL http://www.sciencedirect.com/science/article/pii/S1359645412007203).

[10] M. Cordill, F. Fischer, F. Rammerstorfer, G. Dehm, Adhesion energies of cr thin films on polyimide determined from buckling: experiment and model, Acta Mater. 58 (16) (2010) 5520–5531 (URL http://www.sciencedirect.com/science/article/pii/S1359645410003976).

[11] Effects of substrate compliance on the global unilateral post-buckling of coatings: AFM observations and finite element calculations, Acta Mater. 53 (2) (2005) 441–447 (URL http://www.sciencedirect.com/science/article/pii/S13596 45404005900).

[12] k. Wu, J.Y. Zhang, G. Liu, P. Zhang, P.M. Cheng, J. Li, G.J. Zhang, J. Sun, Buckling behav-iours and adhesion energy of nanostructured cu/x (x = nb, zr) multilayer films on a compliant substrate, Acta Mater. 61 (2013) 7889–7903.

[13] A. Pundt, E. Nikitin, P. Pekarski, R. Kirchheim, Adhesion energy between metal films and polymers obtained by studying buckling induced by hydrogen, Acta Mater. 52 (6) (2004) 1579–1587 (URL http://www.sciencedirect.com/science/article/pii/S13596 45403007389).

[14] M. Hommel, O. Kraft, Deformation behavior of thin copper films on deformable sub-strates, Acta Mater. 49 (19) (2001) 3935–3947 (URL http://www.sciencedirect. com/science/article/pii/S13596 45401002932).

[15] O. Kraft, M. Hommel, E. Arzt, X-ray diffraction as a tool to study the mechanical be-haviour of thin films, Mater. Sci. Eng. A 288 (2) (2000) 209–216 (URL http://www.sciencedirect.com/science/article/pii/S09215 09300008765).

[16] S. Lacour, S. Wagner, Z. Huang, Z. Suo, Stretchable gold conductors on elastomer-ic substrates, Appl. Phys. Lett. 82 (15) (2003) 2404–2406 (URL http://www.scopus.com/inward/record.url?eid=2-s2.0-0037 651101 partnerID=40 md5=95f50c5164836db5d2bdbf4beac8536d).

[17] T. Li, Z. Suo, Deformability of thin metal films on elastomer substrates, Int. J. Solids Struct. 43 (7–8) (2006) 2351–2363 (URL http://www.scopus.com/in-ward/record.url?eid=2-s2.0-3234 4451113 partnerID=40 md5= c145 eff475f7832c8b8c3bec046feab9).

[18] N. Lu, X. Wang, Z. Suo, J. Vlassak, Failure by simultaneous grain growth, strain local-ization, and interface debonding in metal films on polymer substrates, J. Mater. Res. 24 (2) (2009) 379–385 (URL http://www.scopus.com/inward/record.url?eid=2-s2. 0-6174 9101231 partnerID=40 md5=24b297c7a599d3c162401785fa8377d8).

[19] J. Song, Y. Huang, J. Xiao, S. Wang, K. Hwang, H. Ko, D.-H. Kim, M. Stoykovich, J. Rogers, Mechanics of noncoplanar mesh design for stretchable electronic circuits, J. Appl. Phys. 105 (12) (2009) (URL http://www.scopus.com/inward/record.url?eid=2-s2.0-6765 0248647 partnerID=40 md5=2804d95e53c66639b2166d72d91ba905).

[20] Y.-Y. Hsu, M. Gonzalez, F. Bossuyt, F. Axisa, J. Vanfleteren, I. De Wolf, The effects of encapsulation on deformation behavior and failure mechanisms of stretchable interconnects, Thin Solid Films 519 (7) (2011) 2225–2234 (URL http://www.scopus.com/inward/record.url?eid=2-s2.0-7875 1645105 partnerID=40 md5=900be1dd8fb76a1e8b632f4b87be96aa).

[21] K. Lin, J. Chae, K. Jain, Design and fabrication of large-area, redundant, stretch-able interconnect meshes using excimer laser photoablation and in situ masking, IEEE Trans. Adv. Packag. 33 (3) (2010) 592–601 (URL http://www.scopus.com/inward/record.url?eid=2-s2.0-7795 5509627 partnerID=40 md5=41b7f3929cb0bd4d54018c5196d4924b).

[22] D. Brosteaux, F. Axisa, M. Gonzalez, J. Vanfleteren, Design and fabrication of elastic interconnections for stretchable electronic circuits, IEEE Electron Device Lett. 28 (7) (2007) 552–554 (URL http://www.scopus.com/inward/record.url?eid=2-s2.0-3444 7274277 partnerID=40 md5=74cfc8928fe2c78204678330612ef859).

[23] K. Lin, K. Jain, Design and fabrication of stretchable multilayer self-aligned inter-connects for flexible electronics and large-area sensor arrays using excimer laser photoablation, IEEE Electron Device Lett. 30 (1) (2009) 14–17 (URL http://www.scopus.com/inward/record.url?eid=2-s2.0-5814 9528226 partnerID=40 md5=e42e4fb7f5da7df69ab83da60c41911a).

[24] D.S. Gray, J. Tien, C.S. Chen, High-conductivity elastomeric electronics, Adv. Mater. 16 (5) (2004) 393–397 (URL http://dx.doi.org/10.1002/adma.200306107).

[25] N. Lu, C. Lu, S. Yang, J. Rogers, Highly sensitive skin-mountable strain gauges based entirely on elastomers, Adv. Funct. Mater. 22 (19) (2012) 4044–4050 (URL http://doi.org/10.1002/adfm.201200498).

[26] D. Kim, J. Xiao, J. Song, Y. Huang, J. Rogers, Stretchable, curvilinear electronics based on inorganic materials, Adv. Mater. 22 (19) (2010) 2108–2124 (URL http://www.scopus.com/inward/record.url?eid=2-s2.0-7795 2993872 partnerID=40 md5=b2245d5cb8abf50c72bdd5b710931d3e).

[27] A. Siegel, S. Phillips, M. Dickey, N. Lu, Z. Suo, G. Whitesides, Foldable printed circuit boards on paper substrates, Adv. Funct. Mater. 20 (1) (2010) 28–35 (URL http://www.scopus.com/inward/record.url?eid=2-s2.0-7624 9088043 partnerID=40 md5=e132d09d08db546b25cf0bb7a2fb6bdc).

[28] S. Lacour, J. Jones, S. Wagner, T. Li, Z. Suo, Stretchable interconnects for elastic electronic surfaces, Proc. IEEE 93 (8) (2005) 1459–1466 (URL http://www. scopus.com/inward/record.url?eid=2-s2.0-2374 4443567 partnerID=40 md5=08ca34178f3e50e5fc0fb8feae55e9fd).

[29] Y.-Y. Hsu, M. Gonzalez, F. Bossuyt, J. Vanfleteren, I. De Wolf, Polyimide-enhanced stretchable interconnects: design, fabrication, and characteriza-tion, IEEE Electron Device 58 (8) (2011) 2680–2688 (URL http://www.scopus.com/inward/record.url?eid=2-s2.0-7996 0841549 partnerID=40 md5= 57f890254345020efa96e689cbc7413f).

[30] A. Jahanshahi, P. Salvo, J. Vanfleteren, Reliable stretchable gold interconnects in bio-compatible elastomers, J. Polym. Sci. Phys. 50 (11) (2012) 773–776 (URL http://www.scopus.com/inward/record.url?eid=2-s2.0-8486 0181815 partnerID=40 md5=4357440a704ff56a305d506092a689e0).

[31] M. Jablonski, F. Bossuyt, J. Vanfleteren, T. Vervust, H. De Vries, Reliability of a stretchable interconnect utilizing terminated, in-plane meandered copper conductor, Microelectron. Reliab. 53 (7) (2013) 956–963 (URL http://www.scopus. com/inward/record.url?eid=2-s2.0-8487 8473095 partnerID=40 md5= 4c66e32401df62d00836e0e3bb37cdf2).

[32] Y. Zhang, H. Fu, S. Xu, J.A. Fan, K.-C. Hwang, J. Jiang, J.A. Rogers, Y. Huang, A hierar-chical computational model for stretchable interconnects with fractal-inspired de-signs, J. Mech. Phys. Solids 72 (0) (2014) 115–130 (URL http://www.sciencedirect. com/science/article/pii/S00225 09614001495).

[33] Y. Zhang, H. Fu, Y. Su, S. Xu, H. Cheng, J. Fan, K.-C. Hwang, J. Rogers, Y. Huang, Me-chanics of ultra-stretchable self-similar serpentine interconnects, Acta Mater. 61
 (20) (2013) 7816–7827 (URL http://www.scopus.com/inward/record.url?eid=2-s2.0-8488 6284081 partnerID=40 md5=3e810f684f3c2c64cba6c82dd0720cc9).

[34] O. Van Der Sluis, Y. Hsu, P. Timmermans, M. Gonzalez, J. Hoefnagels, Stretching-induced interconnect delamination in stretchable electronic circuits, J. Phys. D. Appl. Phys. 44 (3) (2011) (URL http://www.scopus.com/inward/record.url?eid=2-s2.0-7865 0634811 partnerID=40 md5=9dbd 5319a3539a74e40b8878f56f0da9).

[35] J. Hoefnagels, J. Neggers, P. Timmermans, O. Van Der Sluis, M. Geers, Copper-rubber interface delamination in stretchable electronics, Scr. Mater. 63 (8) (2010) 875–878 (URL http://www.scopus.com/inward/record.url?eid=2-s2.0-7795 5517339
partnerID=40md5=c849d574abb3e51760d7984ad1674493).

[36] N. Lu, X. Wang, Z. Suo, J. Vlassak, Metal films on polymer substrates stretched beyond 50%, Appl. Phys. Lett. 91 (22) (2007) (221909–1–221909–3).

[37] J. Dobrzynska, M. Gijs, Flexible polyimide-based force sensor, Sensors Actuators A Phys. 173 (1) (2012) 127–135 (URL http://www.scopus.com/inward/record.url?eid=2-s2. 0-8465 5166481 partnerID=40 md5=55f4093e1f8ec6ed70c594efb70eeb5d).

[38] W.-Y. Chang, T.-H. Fang, Y.-C. Lin, Physical characteristics of polyimide films for flexible sensors, Appl. Phys. A Mater. 92 (3) (2008) 693–701 (URL http://www. scopus.com/inward/record.url?eid=2-s2.0-4834 9112650 partnerID=40 md5=5b56b8172c9b7135c387311666444178).

[39] J. Jansons, A. Aniskevich, L. Pazhe, Analysis of reversible and irreversible strains in the creep of a nonlinear viscoelastic polymer, Mech. Compos. Mater. 48 (2)(2012) 209–216 (URL http://www.scopus.com/inward/record.url?eid=2-s2.0-8486 3683298 partnerID=40 md5=f21280dd347139419aeb4768f7c862a1).

[40] C.-T. Kuo, M.-C. Yip, K.-N. Chiang, Time and temperature dependent mechanical characterization of polymer-based materials in electronic packaging ap-plications, J. Chin. Inst. Eng. Ser. A 27 (7) (2004) 949–954 (URL http:// www. scopus.com/inward/record.url?eid=2-s2.0-9744 242193 partnerID=40 md5=b0edc8be1b8e3b99720fc21f7ffe5db0).

[41] R. Lucchini, Mechanics of Stretchable Interconnects for Stretchable Electronics Devices(Ph.D. Thesis) Politecnico di Milano, 2014.

[42] J. Goldstein, D.E. Newbury, D.C. Joy, C.E. Lyman, P. Echlin, E. Lifshin, L. Sawyer, J.R. Michael, Scanning Electron Microscopy and X-ray Microanalysis, Springer Science + Business Media, New York, 2003.

[43] J. Field, M. Swain, A simple predictive model for spherical indentation, J. Mater. J. Mater. Res. 8 (2) (1993) 297–306.

[44] D. Tabor, Indentation hardness: fifty years on a personal view, Philos. Mag. A 74 (5)(1996) 1207–1212, http://dx.doi.org/10.1080/01418619608239720 (URL http://dx. doi.org/10.1080/01418619608239720).

[45] S. Chiu, J. Leu, P. Ho, Fracture of metal-polymer line structures. I. Semiflexible polyimide, J. Appl. Phys. 76 (9) (1994) 5136–5142 (URL http://www.scopus. com/inward/record.url?eid=2-s2.0-3644 8999689 partnerID=40 md5= 97be8302e1665ed6b5098b1a6a24f1c5).

[46] Gliding at interface during thin film buckling: a coupled atomistic/elastic approach, Acta Mater. 60 (3) (2012) 1259–1267 (URL http:// www.sciencedirect.com/science/article/pii/S13596 45411008317).